

Synthesis and Biological and Structural Characterization of the Dual-Acting Peroxisome Proliferator-Activated Receptor α/γ Agonist Ragaglitazar

Søren Ebdrup,* Ingrid Pettersson, Hanne B. Rasmussen, Heinz-Josef Deussen, Anette Frost Jensen, Steen B. Mortensen, Jan Fleckner, Lone Pridal, Lars Nygaard, and Per Sauerberg

Novo Nordisk A/S, Novo Nordisk Park, 2760 Måløv, Denmark

Received August 20, 2002

A new and improved synthesis of the peroxisome proliferator-activated receptor (PPAR) agonist ragaglitazar applicable for large-scale preparation has been developed. The convergent synthetic procedure was based on a novel enzymatic kinetic resolution step. The conformation of ragaglitazar bound to the hPPAR γ receptor was quite different compared to the single-crystal structures of the L-arginine salt of ragaglitazar. In particular, the phenoxazine ring system had varying orientations. Ragaglitazar had high affinity for the hPPAR α and γ receptors with IC₅₀ values of 0.98 and 0.092 μ M, respectively. The lack of hPPAR δ activity could be explained by the absence of binding in the tail-up pocket in the hPPAR δ receptor, in contrast to the hPPAR δ agonist GW2433, which was able to bind in both the tail-up and tail-down pockets of the receptor.

Introduction

Type 2 diabetes is a chronic multifactorial metabolic disease characterized by insulin resistance, hyperglycemia, and hyperinsulinemia, leading to impaired secretion of insulin in the later stages. The disease is often associated with obesity, dyslipidemia, and hypertension, leading to increased cardiovascular risks.¹ Owing to the forecasted epidemic in type 2 diabetes, the increasing financial and social costs, and the complicated pathology of the disease, new therapies are needed that address both the insulin resistance and dyslipidemic components of the disease.^{2–4} Different types of PPAR (peroxisome proliferator-activated receptor) agonists have been shown to have beneficial effects on the described characteristics of type 2 diabetes.⁵ Fibrates (PPAR α agonists, e.g., fenofibrate and clofibrate) primarily decrease serum triglyceride levels and increase HDL cholesterol (HDLc) levels, but they also improve glucose tolerance in type 2 diabetic patients.^{5,6} Furthermore, fibrates have been reported to reduce weight gain in rodents without effects on food intake.⁷ Insulin sensitizers (PPAR γ agonists, e.g., pioglitazone (**1**) and rosiglitazone (**2**) (Figure 1)) also have a range of clinical effects including improvement of insulin sensitivity and glucose tolerance and lowering of blood glucose levels in type 2 diabetic patients.^{8,9}

New dual-acting PPAR α and γ agonists, designed to combine the beneficial effects seen with insulin sensitizers and fibrates, have received increased attention. Further, the dual PPAR α and γ agonists might also reduce the weight gain associated with adipogenesis resulting from PPAR γ activation through the simultaneous stimulation of lipid oxidation and decreased adiposity observed after PPAR α activation. Different dual-acting agonists, e.g., ragaglitazar (NNC 61-0029, (-)-DRF 2725, **3**; α , EC₅₀ = 3.2 μ M; γ , EC₅₀ = 0.6 μ M),^{10–12} tesaglitazar (AZ 242, **4**; α , EC₅₀ = 1.2 μ M; γ , EC₅₀ = 1.3 μ M),^{13,14} KRP 297 (**5**; α , EC₅₀ = 1.0 μ M; γ ,

EC₅₀ = 0.8 μ M),¹⁵ and LY465608 (**6**; α , EC₅₀ = 0.15 μ M; γ , EC₅₀ = 0.88 μ M),¹⁶ Figure 1, have recently been described. Ragaglitazar is a selective, potent, and efficacious agonist of the human PPAR α (hPPAR α) and PPAR γ (hPPAR γ) receptors with an α/γ activation ratio of 5.6.¹¹ Clinical phase 2 studies showed significant lowering of plasma triglycerides, total cholesterol, blood glucose, and HbA_{1c} as well as increasing levels of HDL cholesterol at pharmacological relevant doses.^{17,18}

In this paper, an improved and scalable synthetic procedure, which includes an enantioselective enzymatic resolution step, is presented for ragaglitazar. The absolute stereochemistry of ragaglitazar, as well as the crystal structure of the hPPAR γ -ligand binding domain (LBD)-protein complex, is also described. Finally, modeling approaches explaining the hPPAR α , γ , and δ profiles of ragaglitazar are provided.

Chemistry

A novel and improved synthesis of (*S*)-2-ethoxy-3-(4-[2-(phenoxazine-10-yl)ethoxy]phenyl)propanoic acid (*S*-**3**, ragaglitazar) applicable for large-scale production has been developed. The convergent synthetic procedure is based on the condensation of the two key intermediates 2-phenoxazin-10-yl-ethyl methanesulfonate (**12**) and (*S*)-2-propyl 2-ethoxy-3-(4-hydroxyphenyl)propanoate (*S*-**18**) (Scheme 1). The earlier described¹² linear synthesis of ragaglitazar is based on a six-step procedure involving five chromatographic separation steps giving an overall yield of 7% and a chiral purity of 94.6% ee. The optical resolution was performed at the last step in the synthesis as racemic ragaglitazar was converted to a diastereomeric (*S*)-(+)-2-phenylglycinolamide, which was chromatographed and hydrolyzed to give optical pure *S*-**3**.

In the new and improved synthesis of ragaglitazar, enantiomerically pure *S*-**18** was alkylated with the mesylate **12** to give (*S*)-2-propyl 2-ethoxy-3-(4-[2-(phenoxazine-10-yl)ethoxy]phenyl)propanoate (*S*-**19**).¹¹ Alkaline hydrolysis of crude *S*-**19** in 2-propanol with

* To whom correspondence should be addressed. Fax: +45 44663939. Phone: + 45 44434830. E-mail: sebd@novonordisk.com.

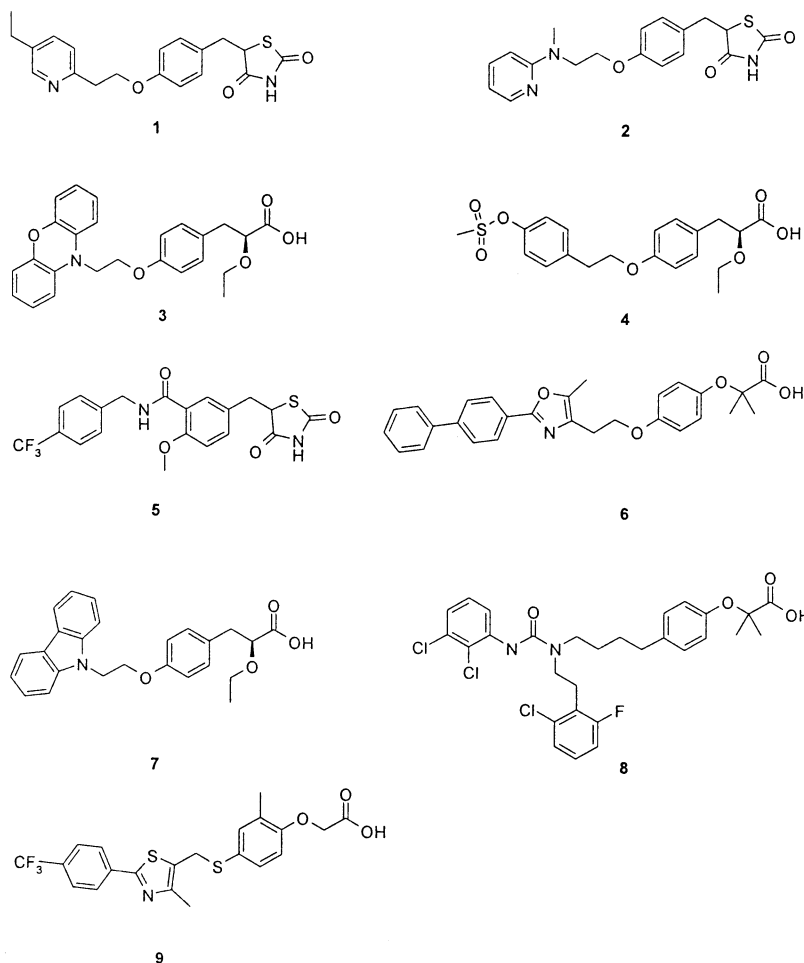


Figure 1. Structures of PPAR agonists: (1) pioglitazone; (2) rosiglitazone; (3) ragaglitazar; (4) tesaglitazar (AZ 242); (5) KRP 297; (6) LY465608; (7) **3q**;¹¹ (8) GW2433; (9) GW501516,

sodium hydroxide yielded (*S*)-2-ethoxy-3-(4-[2-(phenoxazine-10-yl)ethoxy]phenyl)propanoic acid (**S-3**, ragaglitazar) without significant racemization in 81% yield starting from the two key intermediates **12** and **S-18**.

Different approaches to the key intermediate **S-18** have been considered, but because of access to a collection of hydrolases, we decided to investigate if **S-18** could be prepared by enzymatic resolution from racemic ethyl 2-ethoxy-3-(4-hydroxyphenyl)propanoate (*rac*-**16**). More than 80 different hydrolases were initially screened in order to find a highly enantioselective enzyme for this substrate.¹⁹ It was found that racemic *rac*-**16** could be resolved by kinetic resolution with the commercially available enzyme preparation Pectinex Ultra-SP-L from Novozymes A/S. Compound **S-17** was obtained, and the enantiomeric ratio for the process was found to be $E > 200$. The enzymatic process for the preparation of **S-17** has meanwhile been further optimized and scaled and was recently performed on a 44 kg scale.²⁰ *rac*-**16** was prepared from commercially available 4-benzyloxybenzaldehyde (**13**), which was reacted with triethyl 2-ethoxyphosphonoacetate (**14**)²¹ in a Horner–Emmons–Wadsworth²² reaction to give ethyl 3-(4-benzyloxyphenyl)-2-ethoxyacrylate (**15**) as an *E/Z* mixture. **15** was then hydrogenated to ethyl 2-ethoxy-3-(4-hydroxyphenyl)propanoate (*rac*-**16**).

The other key intermediate **12** was prepared from commercially available phenoxazine (**10**) by *N*-alkyla-

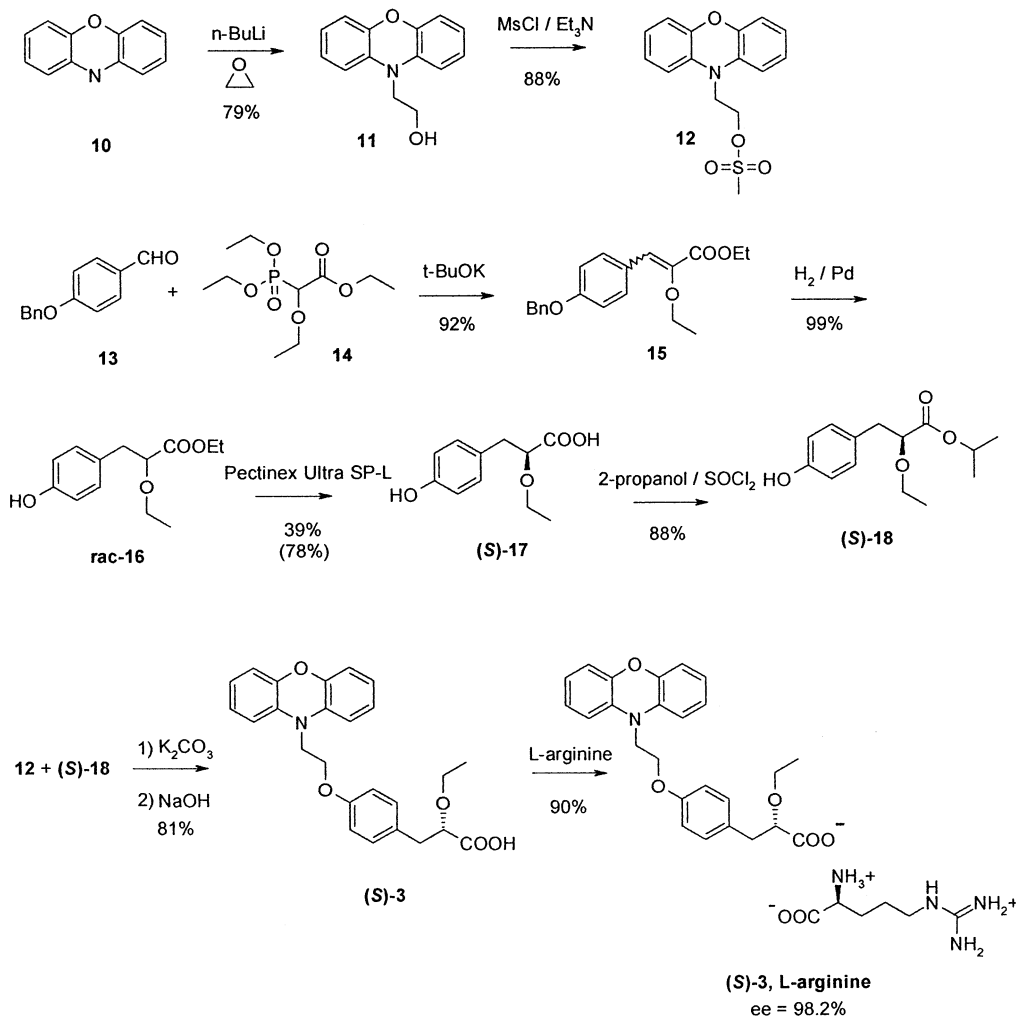
tion with *n*-BuLi/ethylenoxide in *tert*-butyl methyl ether to give 2-phenoxazine-10-yl-ethanol (**11**).^{23,24} The alcohol **11** was then mesylated with methanesulfonyl chloride to give **12**²⁵ in 70% yield over the two steps.

Thus, the overall yield starting from phenoxazine **10** could be improved to 56% with an enantiomeric excess of 98.2%.

To identify a suitable salt of ragaglitazar for pharmaceutical development, various bases that are commonly used in pharmaceutical products (NaOH, KOH, Mg(OH)₂, L-arginine, L-lysine, and *N*-methyl-D-glucamine (meglumine)) were tested for salt formation with the carboxylic acid ($pK_a = 3.7$) of ragaglitazar. The precipitates formed with the bases were subjected to analysis by powder X-ray diffraction, differential scanning calorimetry, and thermogravimetric analysis.²⁶

The L-arginine salt of ragaglitazar (**S-3**, arginine) that was crystallized from ethanol or 2-propanol showed good crystallinity and a melting point suitable for tablet formulation. Moisture sorption studies showed ragaglitazar, L-arginine to be nonhygroscopic. Stability studies at different storage conditions, including elevated temperature and humidity, demonstrated the integrity of the crystal form and satisfactory chemical stability.

On the basis of these results, the L-arginine salt of ragaglitazar was selected as the best candidate for drug development and ragaglitazar was converted to this salt.

Scheme 1. Synthesis of Ragaglitazar, L-Arginine [(*S*)-3, L-Arginine]**Structural Characterization**

The crystal structure of the dimethyl sulfoxide solvate of ragaglitazar, L-arginine was determined by single-crystal X-ray crystallography.^{27,28} The absolute configuration of ragaglitazar was independently determined to be the (*S*)-enantiomer by refining the crystal structure using the anomalous X-ray dispersion from sulfur. This finding is in agreement with the configuration of the active enantiomer of related ligands (e.g., tesaglitazar).¹⁴ The crystal structure contained two crystallographically independent ragaglitazar molecules with different conformations, two identical L-arginine, and two DMSO molecules in the asymmetric unit (Figure 2). The two ragaglitazar molecules (**A** and **B** of Figure 3) had almost identical orientations of the phenylethoxypropanoic acid groups. This moiety could be aligned with a root-mean-square (rms) deviation of 0.12 Å; i.e., the moieties are similar. The conformational difference of the two ragaglitazar molecules could be described as a rotation of the ethoxy-linked phenoxazine group from this moiety. The torsion angles describing this rotation differ by 157(3)° between molecules **A** and **B**.

Binding Studies

Ragaglitazar was further characterized by determining the binding affinity to hPPAR α and γ receptors. The ligand binding assays, using [³H]-ragaglitazar and

[³H]-NNC 61-4655 in the hPPAR γ and α assays, respectively, were further developments of the SPA assay described by Nichols.²⁹ The binding profile of ragaglitazar was compared to the profiles of two marketed insulin sensitizers rosiglitazone and pioglitazone, to the structurally related tesaglitazar, and to the (*R*)-enantiomer of ragaglitazar. Ragaglitazar had the highest affinity for both the hPPAR α (IC₅₀ = 0.98 μ M) and the hPPAR γ receptors (IC₅₀ = 0.092 μ M) of the five compounds tested. The hPPAR γ affinity was considerable higher than the hPPAR γ -selective ligands pioglitazone (7.4 μ M) and rosiglitazone (0.44 μ M), and neither pioglitazone nor rosiglitazone (up to 10 μ M) had affinity for the hPPAR α receptors (Table 1). Tesaglitazar had a binding profile similar to that of ragaglitazar but with lower affinity (Table 1). The *R* isomer of ragaglitazar had less than 10 μ M affinity for both PPAR receptors.

Results and Discussion

In *in vitro* hPPAR α , γ , and δ transactivation assays, ragaglitazar was shown to be a potent and efficacious hPPAR α and hPPAR γ agonist with no hPPAR δ activity (α , EC₅₀ = 3.2 μ M, 97%; γ , EC₅₀ = 0.6 μ M, 117%; δ , 7%).¹¹ Animal studies in db/db mice and high-cholesterol-fed rats further showed that ragaglitazar had excellent blood glucose lowering and insulin sensitizing as well as plasma lipid lowering activities, confirming PPAR α

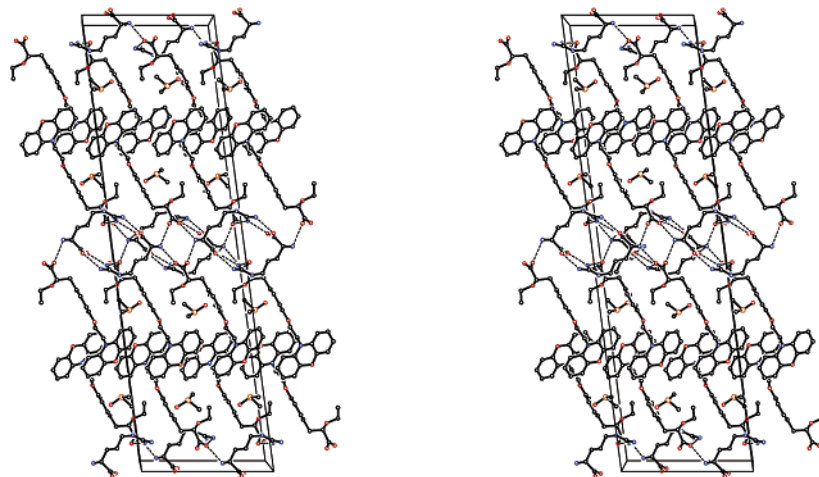


Figure 2. Packing diagram²⁷ in stereo of the ragaglitazar, L-arginine DMSO solvate, showing the unit cell determined by single-crystal X-ray crystallography. The crystallographic *c* axis is horizontal, the *a* axis is inclined to this in the plane of the paper, while the *b* axis is perpendicular to the paper plane. Chemical bonds are indicated by full lines, and hydrogen bonds are indicated by stipulated lines.

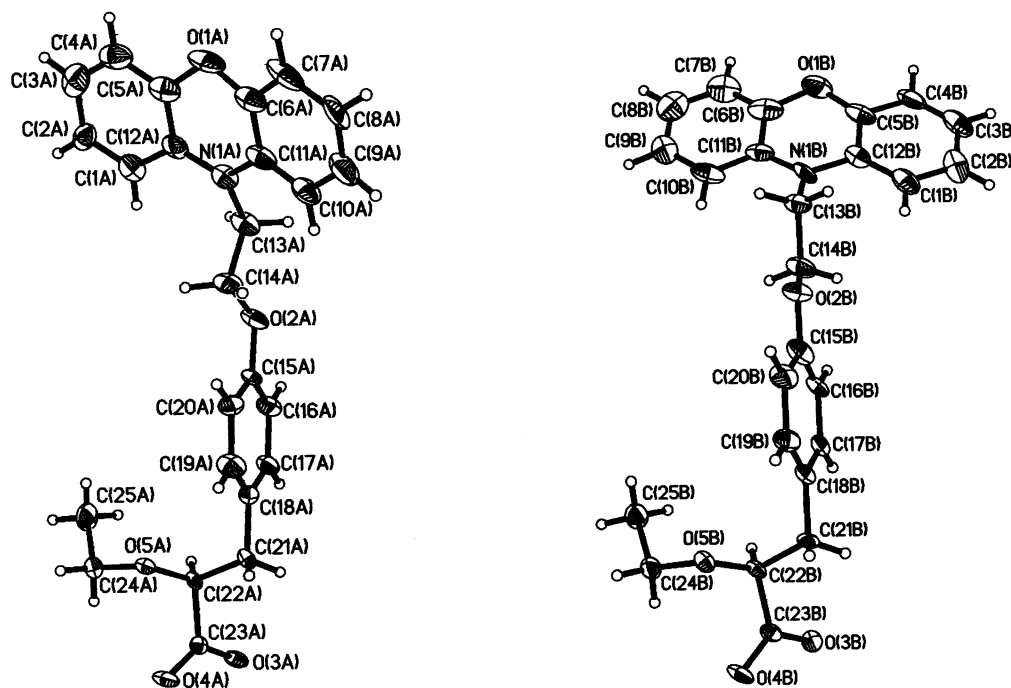


Figure 3. Drawing²⁷ of the two crystallographically independent ragaglitazar molecules A (left) and B (right), determined by single-crystal X-ray crystallography. Thermal ellipsoids are shown at the 50% probability level for non-hydrogen atoms. Hydrogen atoms are shown as small spheres.

Table 1. Receptor Binding Affinities to HPPAR α and γ Receptors of Selected PPAR Agonists

compound	PPAR α ^{a,c} IC ₅₀ , μ M	PPAR γ ^{b,c} IC ₅₀ , μ M
pioglitazone (1)	> 10	7.4 \pm 0.3
rosiglitazone (2)	> 10	0.44 \pm 0.04
ragaglitazar (<i>S</i>) (3)	0.98 \pm 0.04	0.092 \pm 0.003
ragaglitazar (<i>R</i>)	> 10	> 10
tesaglitazar (4)	3.8 \pm 0.3	0.35 \pm 0.04

^a [³H]-NNC 0061-4655 used as radioligand. ^b [³H]-Ragaglitazar used as the radioligand. ^c Results are expressed as the mean \pm SEM (*n* = 5–6).

and PPAR γ activity *in vivo*.¹⁰ Furthermore, clinical phase 1 data with ragaglitazar showed favorable pharmacokinetics in both healthy subjects and type 2 diabetic patients,^{30,31} and phase 2 data confirmed the

animal data showing significant lowering of HbA_{1c} and plasma lipids.^{11,17} Thus, ragaglitazar belongs to a new class of dual PPAR α and γ agonists intended to restore insulin sensitivity and correct dyslipidemia.

To further understand the interaction with the hPPAR γ receptor, crystals of the hPPAR γ -LBD-ragaglitazar complex were prepared by co-crystallization and by soaking. Despite the very different crystallization conditions for the co-crystallized and soaked crystals, the crystals belong to the same space group with similar cell parameters and overall similar structures; only minor differences in the binding of the ligand was detected. The asymmetric unit contained two hPPAR γ -LBD proteins and one ragaglitazar molecule. The overall structure of hPPAR γ -LBD was very similar to the apo structures reported by Nolte et al.³² and Uppenberg et

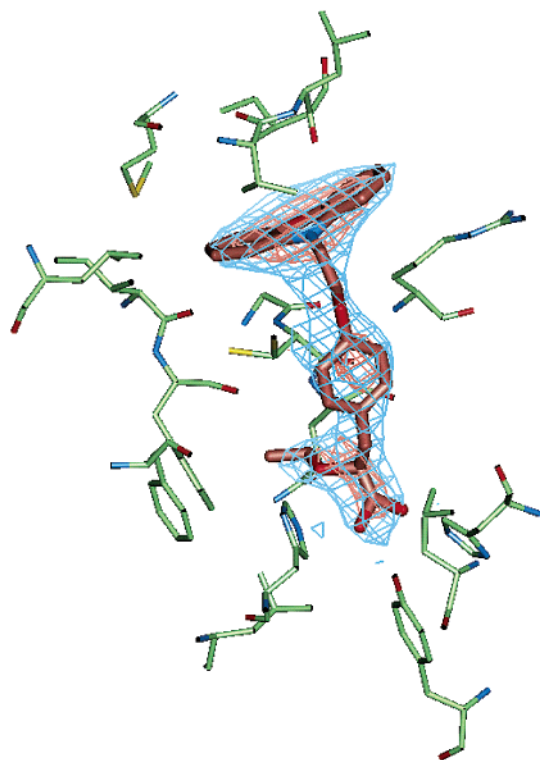


Figure 4. Drawing of the crystal structure of soaked hPPAR γ -LBD in complex with ragaglitazar. The final $2F_0 - F_c$ electron density map covering the ligand is shown at the 1σ level (blue) and 2σ level (orange). The ligand is shown in bold stick, and the coordinating residues of the protein are shown in thin stick.

al.³³ and was similar to the complex structures reported by Oberfield et al.,³⁴ Cronet et al.,¹⁴ and Sauerberg et al.,¹¹ i.e., a homodimer containing one receptor protein in the binding conformation (active) holding a ragaglitazar molecule in the binding site and one receptor protein in the nonbinding conformation (inactive) with an empty binding site.

A close-up examination of the binding pocket, comparing the ragaglitazar complex to the deposited hPPAR γ -LBD apo structures,^{32,33} and the complex structures^{11,14,34} revealed a binding pocket where certain side chains were able to adopt different conformations. In particular, Phe363, Tyr473, and Arg288 showed variations.

The ligands in the two complex structures reported here (soaked and co-crystallized) were placed overall at the same position, with the same relative orientation with respect to the hydrophilic and hydrophobic ends of the ligands (Figure 4). The phenoxazine part, situated in a large hydrophobic cavity of the binding pocket, was oriented slightly differently in the structures based on the co-crystallized and the soaked crystals, indicating that this part of the binding pocket could be explored even further to fully understand its numerous possibilities for ligand accommodation. The different orientations might be explained by the very different crystallization conditions for the co-crystallized specimen relative to the soaked one, both in terms of pH and ionic strength. The possibilities for various orientations in the hydrophobic cavity of the binding pocket were further supported by weak but significant electron density (ed) maps of the phenoxazine moiety in both the co-crystal-

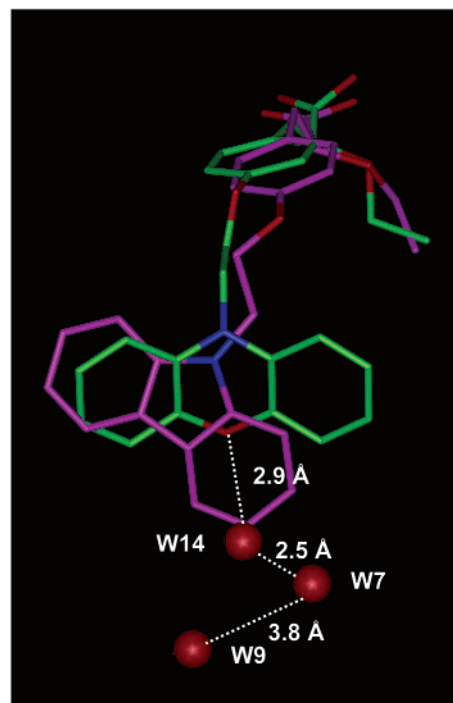


Figure 5. Alignment of ragaglitazar (green carbon atoms) and compound 7 (magenta carbon atoms) in complex with the hPPAR γ receptor.

lized and the soaked structures. Sauerberg et al.¹¹ also reported weak electron density for the carbazole part of 7 (Figure 1).

The structural differences in the binding pocket of the nonbinding receptor protein (inactive) relative to the binding receptor protein (active) were detected in the hydrophilic part coordinating the carboxylic acid moiety of the ligand. Superimposing the active and the inactive receptor proteins showed that His323 and His449 were situated at similar positions while Tyr473 in the inactive receptor was not in place for interaction with the ligand. However, even more striking was that the C-terminal of the inactive receptor was positioned at approximately the same position as the carboxylic acid moiety of the ligand in the active receptor. Not only was the inactive receptor protein lacking a coordinating residue Tyr473 in its binding pocket but also the binding pocket was partly sterically blocked by its own C-terminal residue. The conformation of the nonbinding PPAR γ -LBD monomer might be an effect of crystal packing and not biologically relevant. However, it also shows the receptor to be dynamic in the C-terminal part. Furthermore, the location of the C-terminal in the nonbinding monomer of the receptor shows a strong preference for an acidic group at this position.

To detect hard bound water molecules, which interact with the ligand, and to understand their importance for ligand binding and/or activation of the receptor, Grid calculations with a water probe were performed. In particular, two water molecules (water7 and -14 located in the soaked complex) were found to be of importance (Figure 5). Calculations with a water probe, with the ligand included and water14 excluded, gave an energy minimum close to the position where water14 is located, with an interaction energy of -9.1 kcal/mol. This energy minimum was due to hydrogen bonds to the oxygen atom in the phenoxazine ring system and to water7.

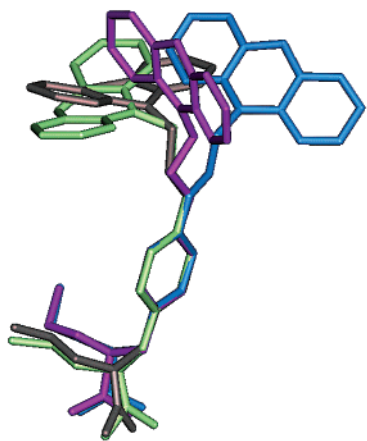


Figure 6. Superimposition based on the phenyl ring of ragaglitazar from four crystal structures: (magenta) conformation A from ragaglitazar, L-arginine single crystal; (cyan) conformation B from ragaglitazar, L-arginine single crystal; (green) conformation from co-crystallized protein structure; (gray) conformation from soaked protein structure.

Calculations with a water probe, with the ligand included and water7 excluded, gave an energy minimum close to that of water7 with a value of -7.4 kcal/mol. This energy minimum was based on a strong hydrogen bond interaction with the oxygen atom in water14 and a weak hydrogen bond with the oxygen atom in water9. The two water molecules (water7 and -14) stabilize the conformation of the hydrophobic moiety observed in the soaked structure. The crystal structure of **7** soaked into the hPPAR γ receptor¹¹ was superimposed with ragaglitazar soaked into the hPPAR γ receptor (Figure 5). In the alignment, the main differences were found in the tricyclic part of the ligands. The carbazole ring system in **7** had no possibility of making hydrogen bonds to water molecules, whereas the phenoxazine ring system in ragaglitazar had this possibility, thus affecting the binding mode of this ligand.

A structural comparison between the apo structure and the two complexes of hPPAR γ -LBD showed that the protein had changed only slightly to make the best fit to ragaglitazar. To study the structural flexibility of the ligand in different environments, the two different conformations of ragaglitazar in the single-crystal structure of the L-arginine salt (**A** and **B**, Figure 3) were compared to the conformations observed in the protein complex crystal structures obtained by soaking and by co-crystallization, respectively. Thus, in total four different molecular conformations of ragaglitazar were observed (Figure 6).

The difference between the four conformations observed for ragaglitazar was to a large extent described by the two torsion angles extending from the ethoxy linker to the phenyl group, C(14x)–O(2x)–C(15x)–C(16x) and C(14x)–O(2x)–C(15x)–C(20x) where x is denoting **A** or **B** in Figure 3. The values for the angles were $170.2(10)^\circ$ and $-8.9(15)^\circ$ for molecule **A** and $13.7(17)^\circ$ and $-167.3(11)^\circ$ for molecule **B** in the ragaglitazar, L-arginine salt crystal, respectively. Thus, the torsion angle differences between molecules **A** and **B** were $157(3)^\circ$ and $158(3)^\circ$ (Figure 6). The corresponding torsion angles for the protein ligands were 73° and -107° for the soaked-in ligand and 70° and -110° for the co-crystallized ligand. The differences between the

Table 2. Alignment of Amino Acids in the Hydrophobic Part of the hPPAR Ligand Binding Domain

PPAR α	PPAR γ	PPAR δ
Ile272	Ile281	Val281
Ala268	Val277	Ile277
Leu347	Leu356	Leu356
Leu247	Leu255	Leu255
Phe343	Phe352	Phe352
Ile241	Ile249	Ile249
Ile339	Met348	Val348
Val332	Ile341	Val341
Met330	Val339	Leu339
Phe359	Phe368	Phe368
Met355	Met364	Ile364
Met325	Met334	Val334
Val324	Leu333	Ile333
Met220	Leu228	Met228
Leu321	Leu330	Leu330
Met320	Met329	Met329
Phe218	Phe226	Phe226

protein ligands for these torsion angles were negligible, but the angles of both ligands differed significantly from the torsion angles of the ragaglitazar, L-arginine salt molecules (Figure 6). The most important difference between the conformations of the two protein ligands was described by the torsion angle extending from the phenoxazine ring to the ethoxy linker N(1x)–C(13x)–C(14x)–O(2x) (Figure 6). This angle was -169° for the soaked-in ligand and -131° for the co-crystallized ligand, a significant difference of 38° . The corresponding values for molecules **A** and **B** in the salt were $-177.1(9)^\circ$ and $175.5(9)^\circ$, which were both quite similar to the soaked-in ligand. The only other major conformational difference between the ragaglitazar, L-arginine salt molecules and the protein ligands was the torsion angle describing the twist of the terminal ethoxy group from the chiral center, C(22x)–O(5x)–C(24x)–C(25x) (Figure 6). This angle was $-78.6(10)^\circ$ and $-77.4(10)^\circ$ for ragaglitazar, L-arginine salt molecules **A** and **B**, respectively, whereas it was 180° and 179° for the soaked-in and the co-crystallized ligands, respectively, i.e., a difference in orientation of approximately 100° . Owing to the conformational differences described above, the relative orientation of the phenyl ring with respect to the phenoxazine ring system differed for the ragaglitazar, L-arginine salt molecules and the protein ligands. The phenyl ring plane was almost parallel to the N(1x)–O(1x) axis in the ragaglitazar, L-arginine salt molecules, whereas this plane was almost perpendicular to the N(1x)–O(1x) axis in the protein ligands (Figure 6). Selected torsion angles are listed in Table S1 (Supporting Information).

In conclusion, a comparison of the structures of ragaglitazar observed in the protein complex to those observed in the single-crystal structure of the ragaglitazar, L-arginine salt showed that the ligand undergoes quite drastic changes dependent on its environment and adapts to the hPPAR γ -LBD protein.

To understand the hPPAR α and γ activity and the lack of hPPAR δ activity for ragaglitazar at a molecular level, the binding pockets in the different receptors were compared. The ligand binding domains of the hPPAR γ , hPPAR α , and hPPAR δ receptors that were crystallized with ragaglitazar (**3**), tesaglitazar (**4**),¹⁴ and GW2433 (**8**)³⁵ (α , EC₅₀ = $0.17 \mu\text{M}$; γ , EC₅₀ = $2.5 \mu\text{M}$; δ , EC₅₀ = $0.19 \mu\text{M}$)⁵ (Figure 1), respectively, were superimposed

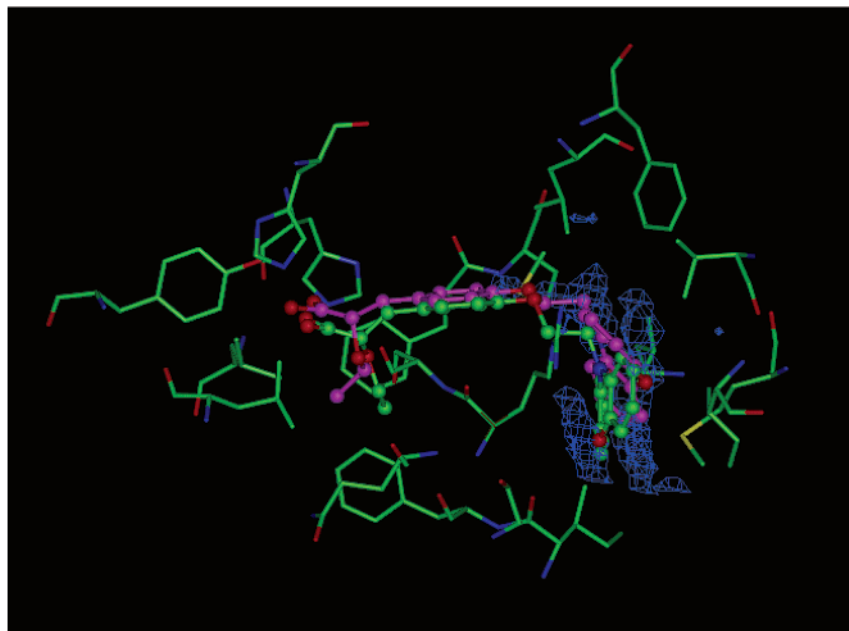


Figure 7. Interactions between a DRY probe (blue grid) and the ligand-binding domain of the hPPAR γ receptor. The amino acids are shown as stick models, and the ligand is shown as a ball-and-stick model. The crystallized ragaglitazar is shown with green carbon atoms, and the FlexX docked ligand is shown with magenta carbon. The amino acids shown are participating in interactions with the ligand.

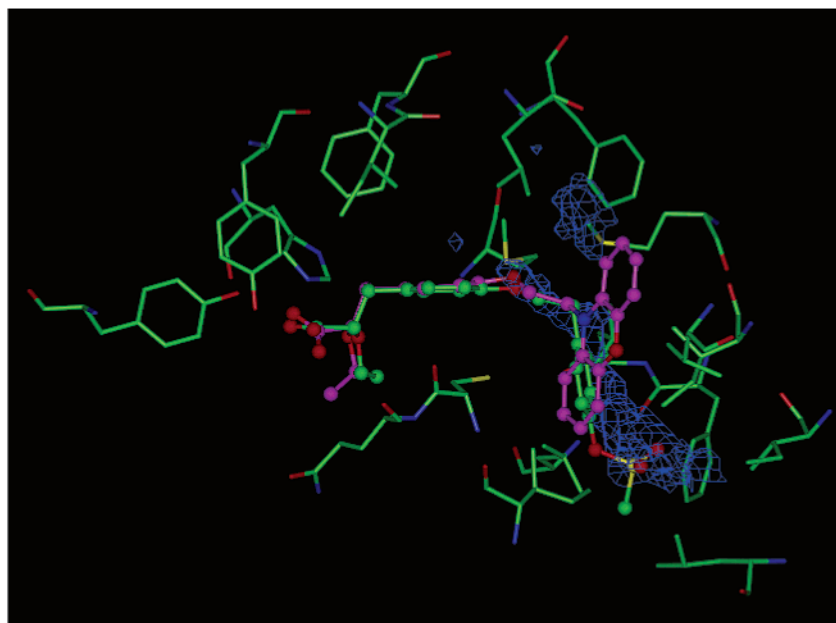


Figure 8. Interactions between a DRY probe (blue grid) and the ligand binding domain of the hPPAR α receptor. The amino acids are shown as stick models, and the ligands are shown as ball-and-stick models. The crystallized tesaglitazar is shown with green carbon atoms and the FlexX docked ragaglitazar is shown with magenta carbon atoms. The amino acids shown are participating in interactions with the ligand.

and the ligands removed. To investigate and compare the characteristics of the hydrophobic pocket, Grid calculations^{36–39} with a DRY (hydrophobic) probe were performed in the part of the pocket that was formed by the amino acids in Table 2. These calculations showed significant differences between the binding pockets (Figures 7–9). The binding pocket in the hPPAR γ receptor showed its main interaction with the DRY probe in the area where the phenoxazine group in ragaglitazar was located (Figure 7). The Grid calculations in the hydrophobic pocket of the hPPAR α receptor showed the same pattern as for the hPPAR γ receptor.

The main interactions were found in the area where the phenyl ring substituted with a methylsulfoxy group was located, (Figure 8). The binding pocket in the hPPAR δ receptor showed two areas in which interactions between the DRY probe and the binding pocket were found (Figure 9). These correspond to the tail-up and tail-down configurations of eicosapentaenoic acid (EPA) crystallized with the ligand binding domain of the hPPAR δ receptor.⁴⁰ The amino acids that formed the hydrophobic pocket in the different receptors are listed in Table 2. One part of the hydrophobic pocket that was found to interact with the DRY probe was common for the

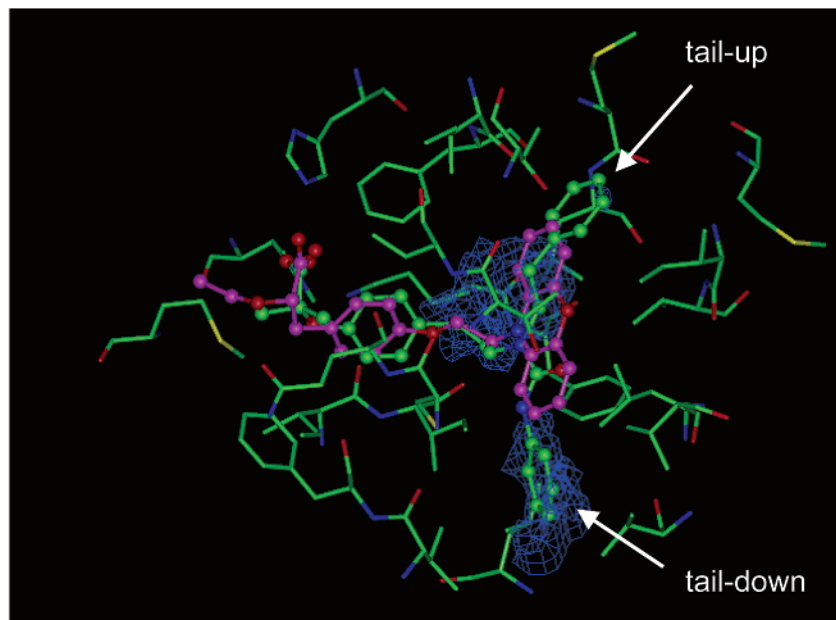


Figure 9. Interactions between a DRY probe (blue grid) and the ligand-binding domain of the hPPAR δ receptor. The amino acids are shown as stick models, and the ligands are shown as ball-and-stick models. The crystallized GW2433 is shown with green carbon atoms, and the FlexX docked ragaglitazar is shown with magenta carbon atoms. The amino acids shown are participating in interactions with the ligand.

Table 3. Results from FlexX Docking of Ragaglitazar, Tesaglitazar, and GW2433

	CScore = 5			CScore = 4		
	no. of solutions	rms, Å	FlexX score	no. of solutions	rms, Å	FlexX score
PPAR γ and ragaglitazar (3)	3	1.9–2.3	–17.1 to –15.5	1	3.4	–12.7
PPAR γ and tesaglitazar (4)	2		–21.6 to –20.4	4		–19.1 to –16.9
PPAR α and tesaglitazar (4)	0			2	0.8–1.3	–16.8 to –16.5
PPAR α and ragaglitazar (3)	2		–23.2 to –22.4	3		–21.5 to –18.8
PPAR δ and GW2433 (8)	2	3.1–6.8	–24.4 to –23.6	3	3.1–6.8	–22.5 to –20.5
PPAR δ and ragaglitazar (3)	1		–16.2	2		–17.5 to –14.1
PPAR δ and GW501516 (9)	4		–26.4 to –24.3	10		–24.5 to –20.7

hPPAR α and the hPPAR γ receptors and the tail-down pocket in the hPPAR δ receptor. The DRY-probe tail-up pocket in the hPPAR δ receptor was not found in the two other receptors. Two of the amino acids in the hPPAR δ receptor that, according to Grid calculations, gave this pocket hydrophobic character (Val334 and Ile364) were substituted with Met325 and Met355 in the hPPAR α receptor and with Met334 and Met364 in the hPPAR γ receptor, which resulted in a different interaction pattern between the DRY probe and the binding pocket.

To further understand the activity of ragaglitazar, FlexX^{41–44} was used to dock ragaglitazar into the binding pockets of the hPPAR α , hPPAR γ , and hPPAR δ receptors. A combination of the rms values to the relevant crystallized ligand, consensus scoring (CScore) values,⁴⁵ and FlexX scores were used to analyze the results (Table 3). To validate the FlexX dockings, ragaglitazar was docked into the crystal structure of the hPPAR γ receptor, tesaglitazar was docked into the crystal structure of the hPPAR α receptor, and GW2433 was docked into the crystal structure of the hPPAR δ receptor (Table 3). The calculations show that FlexX is able to reproduce the experimental binding modes with high CScore values (Table 3). To understand the hPPAR α activity and investigate possible binding modes, ragaglitazar was docked into the hPPAR α receptor (Table 3). FlexX gave solutions with high CScore values and favorable FlexX scores. Ragaglitazar was predicted

to bind to the hPPAR α receptor in a mode similar to that of tesaglitazar (Figure 8). To further validate the predicted binding modes, tesaglitazar was docked into the hPPAR γ receptor (Table 3). This gave solutions with high CScore values and favorable FlexX scores.

To understand the lack of hPPAR δ activity, ragaglitazar was docked into the hPPAR δ receptor (Table 3). When the results from the docking of GW2433 and ragaglitazar into the hPPAR δ receptor were compared (Table 3), docking of ragaglitazar gave fewer solutions with high CScore compared to GW2433 and less favorable FlexX scores. The selective and potent hPPAR δ agonist GW501516 (α , EC₅₀ > 1 μ M; γ , EC₅₀ > 1 μ M; δ , EC₅₀ = 0.001 μ M) (9)⁴⁰ (Figure 1) was also docked into the hPPAR δ receptor (Table 3). This gave high CScore values and favorable FlexX scores. In the proposed docking modes for GW501516, the hydrophobic tail could bind both in the tail-up pocket formed by Phe226, Met228, Met329, Leu330, Ile333, and Val334 and in the tail-down pocket that was formed by Ile249, Leu255, Ile277, Val281, Val341, Val348, Phe352, and Leu356. Thus, on the basis of the FlexX dockings, we propose that the absence of hPPAR δ activity for ragaglitazar can be explained by a lack of favorable interactions between the phenoxazine ring system in ragaglitazar and the hydrophobic part of the binding pocket in the hPPAR δ receptor. Furthermore, on the basis of Grid calculations and the crystal structure of the hPPAR δ receptor

crystallized with GW2433,³⁵ we propose that the hydrophobic part of the binding pocket consists of two pockets and that GW2433 makes interactions with both at the same time as also proposed by Xu et al.³⁵ On the basis of FlexX docking, GW501516 was predicted to be able to bind to either pocket in the hPPAR δ receptor. Because the tail-down pocket is common to all three receptors and since ragaglitazar lacks hPPAR δ activity, we propose that interactions between the tail-up pocket in the hPPAR δ receptor and a ligand are of major importance for hPPAR δ activity.

Conclusion

A new and improved synthesis of ragaglitazar applicable for large-scale preparation was developed. The absolute stereochemistry of ragaglitazar was, not surprisingly, established to be *S*. By comparison of the structures of ragaglitazar, L-arginine in the single crystal to the structures in the hPPAR γ -LBD protein complex, it was shown that the ligand undergoes quite drastic changes to adopt to its environment. Ragaglitazar had high affinity for the hPPAR α and γ receptors, while the lack of hPPAR δ activity could be explained by the absence of binding to the tail-up pocket in the hPPAR δ receptor. The more pronounced hPPAR α activity observed for ragaglitazar and other dual-acting PPAR α and γ agonists gives hope for a new class of drugs with improved properties compared to the known insulin sensitizers (TZDs).

Experimental Section

Chemistry. Melting points were determined either on a capillary melting point apparatus and are uncorrected or on a DSC instrument. NMR data were recorded on a 300 MHz and on a 400 MHz spectrometer. The mass spectrum was recorded on a quadrupole ion trap mass spectrometer with an electrospray ion source (source voltage 3.52 kV, capillary voltage 3.66 V, capillary temperature 175 °C). Elemental analyses were within 0.1% of the calculated values. Enantiomeric purities were determined using capillary electrophoresis performed on a HP^{3D} capillary electrophoresis instrument (80.5/72.0 cm, 50 μ m HP extended light path capillary), Agilent, Waldborn, Germany. The electrolyte used for compounds **S-17** and **S-18** was HS- β -CD (Regis) (2% w/v) and TM- β -CD (SIGMA) (2% w/v) in 24 mM borate buffer, pH 9.3 (HP). The electrolyte used for compounds **3** and **3**, L-arginine was 10%/90% v/v ACN (Rathburn)/(2.0% SB- β -CD (CyDex) and 0.70% DM- β -CD (Agilent) (w/w) in 25 mM phosphate buffer, pH 8.0. The applied voltage was 30 kV. The infrared spectrum was recorded in KBr by a Perkin-Elmer One FTIR IR spectrophotometer equipped with a diffuse reflectance accessory.

Synthesis of Compounds According to Scheme 1. **2-Phenoxazin-10-ylethyl Methanesulfonate, 12.** Triethylamine (24.3 g, 240 mmol) was added to a solution of 2-phenoxazin-10-ylethanol (**11**) (36.0 g, 158 mmol) in dry dichloromethane (180 mL). Methanesulfonyl chloride (22.5 g, 196 mmol) was added dropwise at 5–10 °C. The reaction mixture was then heated to 35 °C for 3 h followed by washing with water (3 \times 150 mL). The organic phase was then dried over MgSO₄ and filtered, and most of the solvent was removed in vacuo. *n*-Hexane (300 mL) was added and the precipitate was filtered and dried in vacuo to yield 42.5 g (88% yield) of the title compound (mp 88–92 °C). ¹H NMR, 400 MHz (acetone-*d*₆): δ 3.11 (s, 3H), 4.06 (t, *J* = 8 Hz, 2H), 4.50 (t, *J* = 8 Hz, 2H), 6.63–6.66 (m, 2H), 6.69–6.72 (m, 2H), 6.79–6.86 (m, 4H). ¹³C NMR (acetone-*d*₆), 100 MHz: δ 37.3, 44.1, 66.4, 113.2, 116.2, 122.4, 124.8, 133.8, 145.6.

Ethyl *E/Z*-3-(4-benzyloxyphenyl)-2-ethoxyacrylate, 15. Triethyl 2-ethoxyphosphonoacetate (**14**) (11.11 g, 41.4 mmol)

was added dropwise to a mixture of *tert*-butyl methyl ether (55 mL) and potassium *tert*-butoxide (4.65 g, 41.4 mmol) under a nitrogen atmosphere at 20–30 °C. 4-Benzyloxybenzaldehyde **13** (4.61 g, 21.7 mmol) was added in portions to this mixture at 5 °C followed by the addition of *tert*-butyl alcohol (6.70 g). The reaction mixture was allowed to reach 15 °C and stirred at this temperature for approximately 30 min, after which the reaction was completed (as judged by TLC). Water (30 mL) was added at 5–10 °C, and the phases were allowed to separate. The organic phase was concentrated in vacuo, and ethanol (30 mL) was added to the stirred solution. After crystallization had occurred, water (18 mL) was added to the suspension. The light-yellow title compound was filtered off, washed with ethanol/water (1:1 v/v), and dried in vacuo to yield 6.52 g (92% yield). ¹H NMR, 400 MHz (acetone-*d*₆): δ 1.12 (t, *J* = 7 Hz), 1.32 (t, *J* = 7 Hz), 1.33 (t, *J* = 7 Hz), 3.91 (q, *J* = 7 Hz), 4.00–3.91 (q, *J* = 7 Hz), 4.12 (q, *J* = 7 Hz), 4.24 (q, *J* = 7 Hz), 5.12 (s), 5.17 (s), 6.10 (s), 6.93 (s), 6.94 (d, *J* = 9 Hz), 7.05 (d, *J* = 9 Hz), 7.15 (d, *J* = 9 Hz), 7.32–7.42 (m), 7.46–7.50 (m), 7.81 (d, *J* = 9 Hz).

Ethyl 2-Ethoxy-3-(4-hydroxyphenyl)propanoate, *rac*-16. Ethyl *E/Z*-3-(4-benzyloxyphenyl)-2-ethoxyacrylate (**15**) (20.0 g, 61.3 mmol) dissolved in *tert*-butyl methyl ether (40 mL) charged with palladium on carbon (5%) (1.0 g, Engelhard Tech code no. 4531) was hydrogenated with vigorous stirring at atmospheric pressure at room temperature for 2–3 days. The catalyst was filtered off and washed with a few milliliters of *tert*-butyl methyl ether. The combined filtrates were concentrated in vacuo to yield 14.5 g (99% yield) of the title compound as a viscous oil, which crystallizes upon standing. ¹H NMR, 400 MHz (acetone-*d*₆): δ 1.09 (t, *J* = 7 Hz, 3H), 1.17 (t, *J* = 7 Hz, 3H), 2.83–2.91 (m, 2H), 3.35 (dq, *J* = 7 and 14 Hz, 1H), 3.55 (dq, *J* = 7 and 14 Hz, 1H), 3.98 (dd, *J* = 4.7 Hz, 1H), 4.10 (q, *J* = 7 Hz, 2H), 6.74 (d, *J* = 9 Hz, 2H), 7.06 (d, *J* = 9 Hz, 2H), 8.08 (s, 1H). ¹³C NMR (acetone-*d*₆), 100 MHz: δ 4.9, 15.9, 39.5, 61.3, 66.6, 81.5, 116.2, 129.3, 131.6, 157.3, 173.0.

(*S*)-2-Ethoxy-3-(4-hydroxyphenyl)propanoic Acid, S-17. Ethyl 2-ethoxy-3-(4-hydroxyphenyl)propanoate (50.0 g, 210.0 mmol) (*rac*-**16**) was mixed with an aqueous phosphate buffer, pH 7.0 (0.1 M, 100 mL). Pectinex Ultra SP-L (Novozymes A/S, Denmark) (150 mL) was added, and the mixture was stirred vigorously for approximately 44 h at room temperature. During that time, the pH of the reaction mixture was kept constant at pH 6.5–7.5 by addition of NaOH (5 M, 19.0 mL). After 45% conversion, most of the water was evaporated in vacuo (approximately 200 mL) and methanol (500 mL) was added to the remaining slurry. The precipitate that formed was filtered off, and the methanol was evaporated in vacuo. The remaining oil was dissolved in water (150 mL) followed by extraction of the unreacted ester with *tert*-butyl methyl ether (4 \times 100 mL). The water phase was acidified to pH 3 and extracted with *tert*-butyl methyl ether (3 \times 150 mL). After the mixture was dried over Na₂SO₄ and after evaporation of the solvent, 17.0 g (39%) of the title compound was obtained as an oil that crystallized on standing (mp 105 °C, ee = 99.6%). ¹H NMR, 400 MHz (acetone-*d*₆): δ 1.10 (t, *J* = 7 Hz, 3H), 2.85 (dd, *J* = 7 and 14 Hz, 1H), 2.96 (dd, *J* = 4 and 14 Hz, 1H), 3.37 (dq, *J* = 7 and 14 Hz, 1H), 3.62 (dq, *J* = 7 and 14 Hz, 1H), 4.01 (dd, *J* = 4.7 Hz, 1H), 6.74 (d, *J* = 8 Hz, 2H), 7.10 (d, *J* = 8 Hz, 2H). ¹³C NMR (acetone-*d*₆), 100 MHz: δ 15.4, 38.9, 66.4, 80.8, 115.8, 129.3, 131.2, 156.9, 173.5.

(*S*)-2-Propyl 2-Ethoxy-3-(4-hydroxyphenyl)propanoate, S-18. (*S*)-2-Ethoxy-3-(4-hydroxyphenyl)propanoic acid (**S-17**) (16.52 g, 78.6 mmol) was dissolved in dry 2-propanol (80 mL). Thionyl chloride (9.35 g, 78.6 mmol) was added slowly to this solution at room temperature. The mixture was heated to 60 °C and stirred for 2 h at this temperature. The solvent was distilled off, and the remainder was dissolved in *tert*-butyl methyl ether (100 mL). The solution was washed with aqueous NaHCO₃ (10%, 2 \times 50 mL), dried over Na₂SO₄, and filtered, and the solvent was removed in vacuo. A yield of 17.45 g (88%) of the title compound was obtained as an oil, which crystallized on standing (ee = 99.4%). ¹H NMR, 400 MHz (acetone-*d*₆): δ 1.10 (t, *J* = 7 Hz, 3H), 1.12 (d, *J* = 6 Hz, 3H), 1.19 (d, *J* = 6

Hz, 3H), 2.84–2.87 (m, 2H), 3.36 (m, 1H), 3.55 (m, 1H), 4.94 (m, 1H), 6.74 (d, $J = 8$ Hz, 2H), 7.07 (d, $J = 8$ Hz, 2H). ^{13}C NMR (acetone- d_6), 75 MHz: δ 15.9, 22.3, 22.4, 39.4, 66.5, 68.8, 81.6, 116.1, 129.3, 131.6, 157.3, 172.6.

(S)-2-Ethoxy-3-(4-[2-(phenoxazine-10-yl)ethoxy]phenyl)propanoic Acid, S-3. A mixture of 2-phenoxazin-10-ylethyl methanesulfonate (**12**) (12.80 g, 41.9 mmol), potassium carbonate (8.70 g, 62.9 mmol), and toluene (65 mL) was heated to reflux. (S)-2-Propyl 2-ethoxy-3-(4-hydroxyphenyl)propanoate (**S-18**) (10.10 g, 40.0 mmol) dissolved in toluene (30 mL) was added dropwise over 2 h, and the mixture was then refluxed for 20 h. The reaction mixture was cooled to room temperature, and water (50 mL) was added. The organic phase was separated and washed with acetic acid (5%, 50 mL). Evaporation of the solvent in vacuo yielded crude (S)-2-propyl 2-ethoxy-3-(4-[2-phenoxazine-10-yl]ethoxy]phenyl)propanoate (**S-19**), which was dissolved in a mixture of water (35 mL) and 2-propanol (35 mL). Aqueous sodium hydroxide (30%, 12 g) was added, and the mixture was stirred vigorously for 16 h at room temperature. Toluene (50 mL) and fumaric acid (5 g) were added to the mixture, and the organic phase was separated. The organic phase was washed with brine (20 mL), dried over Na_2SO_4 , decolorized with charcoal, and filtered. The title compound was then crystallized by addition of *n*-heptane. The crystalline title compound was filtered off and dried in vacuo to give 13.59 g (81%) of the title compound (mp 89–90 °C, ee = 98.2%). 46 ^1H NMR, 300 MHz (acetone- d_6): δ 1.09 (t, $J = 7$ Hz, 3H), 2.87 (dd, $J = 8$ and 14 Hz, 1H), 2.98 (dd, $J = 5$ and 14 Hz, 1H), 3.36 (dq, $J = 7$ and 14 Hz, 1H), 3.62 (dq, $J = 7$ and 14 Hz, 1H), 4.01 (dd, $J = 5.7$ Hz, 1H), 4.06 (t, $J = 6$ Hz, 2H), 4.27 (t, $J = 6$ Hz, 2H), 6.60–6.71 (m, 4H), 6.80–6.86 (m, 4H), 6.86 (d, $J = 9$ Hz, 2H), 7.18 (d, $J = 9$ Hz, 2H). ^{13}C NMR (acetone- d_6), 75 MHz: δ 15.8, 39.2, 45.2, 65.5, 66.8, 80.9, 113.8, 115.4, 116.34, 122.4, 125.1, 131.4, 131.7, 134.7, 146.0, 158.7. Anal. ($\text{C}_{25}\text{H}_{25}\text{NO}_5$) C, H, N.

L-Argininium (2S)-2-Ethoxy-3-(4-[2-(10H-phenoxazine-10-yl)ethoxy]phenyl)propanoate, S-3, L-Arginine. (S)-2-Ethoxy-3-(4-[2-(phenoxazine-10-yl)ethoxy]phenyl)propanoic acid (**S-3**) (12.00 g, 28.6 mmol) was dissolved in ethanol (260 mL), and the solution was filtered. L-Arginine (4.98 g, 28.6 mmol) dissolved in water (35 mL) at 50–60 °C was added dropwise to the ethanol solution at 75–78 °C with stirring. The solution was slowly cooled to room temperature overnight and finally to 0–5 °C with vigorous stirring. The crystalline precipitate was filtered off, washed with ethanol (2 \times 30 mL), and dried in vacuo to give 15.28 g (90%) of the title compound as an off-white powder (mp 180 °C (DSC), ee = 98.2%). Anal. ($\text{C}_{31}\text{H}_{39}\text{N}_5\text{O}_7$) C, H, N. IR (KBr), cm^{-1} : 3240, 3063, 2971, 2871, 3500–2500 br, 2643, 1708, 1688, 1615, 1587, 1510, 1489, 1374, 1347, 1312, 1273, 1244, 1129, 1045. MS m/z : 420 (MH^+). ^1H NMR, 400 MHz (dms- d_6): δ 0.97 (t, $J = 7$ Hz, 3H), 1.57 (m, 2H), 1.65 (m, 1H), 1.75 (m, 1H), 2.64 (dd, $J = 14$ and 8.5 Hz, 1H), 2.82 (dd, $J = 14$ and 4 Hz, 1H), 3.05 (m, 2H), 3.14 (dq, $J = 9$ and 7 Hz, 1H), 3.23 (t, $J = 5.5$ Hz, 1H), 3.52 (dq, $J = 9.7$ Hz, 1H), 3.59 (dd, $J = 4$ and 8.5 Hz, 1H), 3.99 (t, $J = 6$ Hz, 2H), 4.17 (t, $J = 6$ Hz, 2H), 6.64 (m, 2H), 6.67 (m, 2H), 6.82 (m, 2H), 6.83 (m, 2H), 6.79 (d, $J = 8.5$ Hz, 2H), 7.11 (d, $J = 8.5$ Hz, 2H), 7.90 (br. s, 8H). ^{13}C NMR (DMSO- d_6), 100 MHz: δ 15.1, 24.6, 28.5, 38.3, 40.3, 43.5, 53.5, 63.8, 64.1, 81.9, 112.5, 113.8, 114.9, 121.0, 123.9, 130.0, 132.1, 132.9, 143.9, 156.3, 157.5, 171.5, 175.7. Powder XRD diffractogram is given in Supporting Information. $pK_a = 3.7$. Solubility in water is greater than 40 mg/mL.

Crystallization of Ragaglitazar, L-Arginine. Growth of single crystals of the ragaglitazar, L-arginine salt from solution in 2-propanol or ethanol was not successful. Therefore, ragaglitazar, L-arginine (28 mg) was dissolved in dimethyl sulfoxide (0.3 mL) and large (up to 0.5 mm) plate-shaped (0.01 mm thick) single crystals suitable for X-ray diffraction were grown by slow evaporation at 40 °C over 1–2 days. Crystal data are listed in Supporting Information.

Expression and Purification of hPPAR γ -LBD. A full-length hPPAR γ cDNA was obtained by PCR amplification using cDNA synthesized by reverse transcription of mRNA

from adipose tissue using the following primers: sense, 5'-TGCATCGACATGACCATGGTTGACACAGAG-3'; antisense, 5'-TCAGTCTAGACTAGTACAAGTCCTTGATAGAT-3'. Amplified cDNAs were cloned into pCR2.1-TOPO (Invitrogen) and sequenced. For expression in *E. coli*, the ligand binding domain (LBD, amino acids C₁₆₅ – Stop) of hPPAR γ was generated by PCR using the primers (sense) 5'-Gatcggatcctctcacacaac-gcattcgtttt-3' and (antisense) 5'-TCAGTCTAGACTAGTACAAGTCCTTGATAGAT-3' and fused in frame to glutathione S-transferase in the vector pGEX-3X (Amersham Pharmacia Biotech). The ensuing construct was verified by sequencing. A 5 mL culture inoculated with *E. coli* harboring this construct was grown overnight at 37 °C. After dilution (1:100) and regrowth to OD₆₀₀ = 0.5, the culture was cooled to 25 °C. Recombinant protein was produced by adding IPTG to the culture to a final concentration of 0.1 mM.

Cells were harvested and resuspended in 50 mM imidazole, pH 7.2, 5 mM EDTA, 10% glycerol, 0.1% PMSF, 0.1% DNase, and 0.1% MgCl_2 . After stirring for 1 h, the cells were broken by cell disruption at 150 bar. The material was frozen, thawed, and centrifuged at 40000g for 30 min. The supernatant was loaded on a GSH-Sepharose column (Pharmacia) in 50 mM imidazole, pH 7.2, 1 mM EDTA, 10% glycerol, and 150 mM NaCl and eluted with 250 mM imidazole, pH 7.0, and 300 mM NaCl. The material was subjected to factor Xa digestion (10 units FXa/mg protein) for 16 h. Cleaved GST protein was removed by passage over a GSH-Sepharose column. The hPPAR γ -LBD was further purified by Superose 200 size exclusion chromatography (Pharmacia) in 20 mM Tris, pH 8.0, 0.5 mM EDTA, 5 mM DTT. After SDS-PAGE and MALDI-TOF MS analysis, fractions containing hPPAR γ -LBD were pooled and concentrated by Centricon-30 (Amicon) to 15 mg/mL. N-terminal sequencing verified the cleaved protein to consist of a.a. 188–476.

Crystallization of the hPPAR γ -LBD–Ragaglitazar Complex. Crystals of the hPPAR γ -LBD–ligand complex were produced in two different ways: by co-crystallization and by soaking.

1. Co-crystallization. The free acid form of the ligand ragaglitazar was dissolved in DMSO and mixed with hPPAR γ -LBD in a molar ratio of 3:1. The mixture was left for 60 min before crystallization setup. Crystals were grown by the sitting drop vapor diffusion method, mixing equal amounts of hPPAR γ -LBD–ragaglitazar and reservoir (0.1 M Tris buffer, pH 7.0, 30% PEG monomethylether (mme) 5000, and 0.5 M ammonium sulfate). The final concentration of DMSO in the drop was 1% due to the ragaglitazar solution. Crystals grew to a size of 0.15 mm \times 0.15 mm \times 0.02 mm over 14 days. Crystals were flash-frozen at 100 K prior to data collection. Cryoconditions were 35% PEGmme 5000, 0.1 M Tris, pH 7, and 0.2 M ammonium sulfate including ragaglitazar. Diffraction data to 2.9 Å resolution were collected at beamline 711⁴⁷ equipped with a Mar345 image plate detector at the MAX-lab synchrotron facilities. Data processing and reduction were performed using the programs DENZO and SCALEPACK.⁴⁸ Cell parameters, space group, and data statistics are listed in Table S2 (Supporting Information).

2. Soaked Crystals. Crystals of the apo protein were grown using the sitting drop vapor diffusion method at slightly modified conditions reported by Nolte et al.³² Crystals were grown by mixing equal amounts of hPPAR γ -LBD and reservoir solution (0.8 M sodium citrate and 0.15 M Tris, pH 8.0). Within 10 days, crystals grew to a size of 0.15 mm \times 0.15 mm \times 0.1 mm. The ligand was introduced to the drop by addition of 0.15 μL of 1 mM arginine salt of ragaglitazar dissolved in water. The crystals were left to soak for 10 days. Crystals were flash-frozen at 100 K prior to data collection. Cryoconditions were 40% glycerol, 0.6 M sodium citrate, and 7% PEGmme 5000 including the arginine salt of ragaglitazar. Diffraction data to 2.65 Å resolution were collected on a Mar345 image plate detector mounted at a Rigaku RU-300 rotating anode generator. Data processing and reduction were performed using the programs DENZO and SCALEPACK.⁴⁸ Cell parameters, space

group, and data statistics are listed in Table S2 (Supporting Information).

Structure Determination of the hPPAR γ -LBD–Ragaglitazar Complex. Both structures were solved by the molecular replacement method with the apo hPPAR γ -LBD structure 1PRG (Nolte et al.³²) as search model using the program AMORE.^{49,50} Refinement was performed using the programs X-PLOR⁵¹ and CNX⁵² and model building with the program Quanta (Molecular Simulations). Parameter and topology files were generated using the program Xplo2D.⁵³ Refinement statistics are listed in Table S3 (Supporting Information). After an initial cycle of refinement and model building, the ligand was introduced in the $F_o - F_c$ difference electron density (ed) map. Water molecules were introduced in the structure based on the diffraction data from the soaked crystals using a 2.5σ cutoff in the $F_o - F_c$ difference ed map. The coordinates have been deposited in the Brookhaven Protein Data Bank, ID 1NXX.

Modeling. The ligand binding domains of hPPAR α , hPPAR γ , and hPPAR δ were superimposed with the backbone atoms in the amino acids shown in Table 2, Tyr314 and His440 (PPAR α), His323 and His449 (PPAR γ), and His323 and His449 (PPAR δ). The rms between the hPPAR α and hPPAR γ receptors was 0.67 Å, and the rms between hPPAR δ and hPPAR γ receptors was 0.65 Å.

The Grid calculations were performed with Grid, version 20,^{36–38} with DPRO equal to 4, DWAT equal to 80, and EMAX equal to 5. The calculations with the DRY probe were performed with two planes per ångström and with the water probe with five planes per ångström. All calculations on the complexes between ragaglitazar and the hPPAR γ receptor were performed using the structure based on soaked crystals.

FlexX version 1.10.0 was used.^{41–44} Assignment of formal charges in the ligands was used. Consensus scoring was applied on the obtained solutions.⁴⁵ FlexX was used with the Sybyl 6.8 interface.⁵⁴

The ligands used for docking were built with Maestro 4.1,⁵⁵ and the global energy minimum was found using MacroModel 7.2⁵⁶ and the SUMM method.⁵⁷ The calculations were performed with the MMFF force field^{58–64} and with water as the solvation model.⁶⁵

Binding Assays. The hPPAR binding assay described by Nichols et al.²⁹ was used with a few minor adjustments. The ligand binding assays were based on SPA (scintillation proximity assay) particles.

Ragaglitazar ($K_d = 85$ nM) and NNC 61-4655 ($K_d = 175$ nM) were labeled with ³H and used as a tracer for the receptors GST-PPAR γ -LBD and HIS-PPAR α -LBD, respectively. [³H]-Ragaglitazar was prepared by tritiation of an acrylic acid precursor,⁶⁶ and [³H]-NNC 61-4655 was prepared by catalytic tritium dehalogenation of an aryl bromide precursor.⁶⁷

Acknowledgment. We are indebted to Centre for Crystallographic Studies, University of Copenhagen, for collection of X-ray diffraction data from the ragaglitazar, L-arginine salt single crystal. We gratefully acknowledge useful discussions and technical support from Dr. Reddy Research Foundation, India, and Siegfried CMS LTD, Switzerland. The preparation of [³H] tracers by J. B. Kristensen and S. K. Johansen and the preparation of the ragaglitazar, L-arginine salt by Petra Wiede Lugstein are gratefully acknowledged. The technical assistance from K. M. Klausen, V. Weil, F. Gundertofte, A. Hansen, and A. Ryager, Novo Nordisk A/S, is highly appreciated. Scientific assistance from and fruitful discussions with M. Zundel, H. Olsen, and I. T. Christensen at Novo Nordisk A/S and with P. Østergaard at Novozymes A/S is also gratefully acknowledged.

Supporting Information Available: Crystallographic data and analysis for the single crystal of ragaglitazar, L-arginine, comparison of torsion angles in the ragaglitazar,

L-arginine salt molecules and the protein ligands (Table S1), data collection for the co-crystallized and soaked hPPAR γ -LBD crystal (Table S2), statistical data for the co-crystallized and soaked hPPAR γ -LBD crystal (Table S3), and powder X-ray diffraction results (Figure S1). This material is available free of charge via the Internet at <http://pubs.acs.org>.

References

- Ginsberg, H.; Plutzky, J.; Sobel, E. Review of metabolic and cardiovascular effects of oral antidiabetic agents: beyond glucose-lowering. *J. Cardiovasc. Risk* **1999**, *6* (5), 337–346.
- Cobb, J.; Dukes, I. Recent Advances in the Development of Agents for Treatment of Type 2 Diabetes. *Annu. Rep. Med. Chem.* **1998**, *33*, 213–221.
- Grover, S. A.; Coupal, L.; Zowall, H.; Dorais, M. Cost-Effectiveness of Treating Hyperlipidemia in the Presence of Diabetes. *Circulation* **2000**, *102*, 722–727.
- Bailey, C. J. Potential new treatments for type 2 diabetes. *TIPS* **2000**, *21*, 259–265.
- Willson, T. M.; Brown, P. J.; Sternbach, D. D.; Henke, B. R. The PPARs: From orphan receptors to drug discovery. *J. Med. Chem.* **2000**, *43*, 527–550.
- Staels, B.; Dallongeville, J.; Auwerx, J.; Schoonjans, K.; Leitersdorf, E.; Fruchart, J.-C. Mechanism of Action of Fibrates on Lipid and Lipoprotein Metabolism. *Circulation* **1998**, *98*, 2088–2093.
- Chaput, E.; Saladin, R.; Silvestre, M.; Edgar, A. D. Fenofibrate and Rosiglitazone Lower Triglycerides with Opposing Effects on Body Weight. *Biochem. Biophys. Res. Commun.* **2000**, *271*, 445–450.
- Boyle, P. J.; King, A. B.; Olansky, L.; Marchetti, A.; Lau, H.; Magar, R.; Martin J. Effects of Pioglitazone and Rosiglitazone on Blood Lipid Levels and Glycemic Control in Patients with Type 2 Diabetes Mellitus: A Retrospective Review of Randomly Selected Medical Records. *Clin. Ther.* **2002**, *24* (3), 378–396.
- Chilcott, J.; Tappendem, P.; Jones, M. L.; Wight, J. P. A Systematic Review of the Clinical Effectiveness of Pioglitazone in the Treatment of Type 2 Diabetes Mellitus. *Clin. Ther.* **2001**, *23*, 1792–1823.
- Wulff, E. M.; Jeppesen, L.; Bury, P. S.; Mogensen, J. P.; Fleckner, J.; Andersen, A.-S. T.; Wassermann, K.; Sauerberg, P.; Characterisation of a Future Generation Insulin Sensitizers in Vitro and in Vivo. *Diabetes* **2001**, *50* (Suppl. 2), A524.
- Sauerberg, P.; Pettersson, I.; Jeppesen, L.; Bury, P. S.; Mogensen, J. P.; Wasserman, K.; Brand, C. L.; Sturis, J.; Wöldike, H. F.; Fleckner, J.; Andersen, A.-S. T.; Mortensen, S. B.; Svensson, L. A.; Rasmussen, H. B.; Lehman, S. V.; Polivka, Z.; Sindelar, K.; Panajotova, V.; Ynddal, L.; Wulff, E. M. J. Novel tricyclic- α -alkyloxyphenylpropionic acids: Dual PPAR α/γ agonists with hypolipidemic and antidiabetic activity. *J. Med. Chem.* **2002**, *45*, 789–804.
- Lohray, B. B.; Lohray, V. B.; Bajji, A. C.; Kalchar, S.; Poondra, R. R.; Padakanti, S.; Chakrabarti, R.; Vikramadithyan, R. K.; Misra, P.; Juluri, S.; Namidi, N. V. S. R.; Rajagopalan, R. (–)-3-[4-[2-(phenoxazine-10-yl)ethoxy]phenyl]-2-ethoxypropanoic acid [(–)DRF 2725]: A Dual PPAR Agonist with Potent Antihyperglycemic and Lipid Modulating Activity. *J. Med. Chem.* **2001**, *44*, 2675–2678.
- Kjellstedt, A.; Oakes, N.; Svensson, L.; Carlson, A.-C.; Ljung, B. AZ 242, a Novel PPAR α/γ Agonist, Has Potent and Efficient Insulin-Sensitizing and Antidyslipidemic Properties in ob/ob Mice and fa/fa Zucker Rats. *Diabetes* **2001**, *50* (Suppl. 2), A121.
- Cronet, P.; Petersen, J. F. W.; Folmer, R.; Blomberg, N.; Sjöblom, K.; Karlsson, U.; Lindstedt, E.-L.; Bamberg, K. Structure of the PPAR α and γ ligand binding domain in complex with AZ 242: Ligand selectivity and agonist activation in the PPAR family. *Structure* **2001**, *9*, 699–706.
- Murakami, K.; Tobe, K.; Ide, T.; Mochizuki, T.; Ohashi, M.; Akanuma, Y.; Yazaki, Y.; Kadowaki, T. A Novel Insulin Sensitizer Acts as a Coligand for Peroxisome Proliferator-Activated Receptor- α (PPAR- α) and PPAR- γ . Effects of PPAR- α Activation on Abnormal Lipid Metabolism in Liver of Zucker Fatty Rats. *Diabetes* **1998**, *47*, 1841–1847.
- Etgen, G. J.; Oldham, B. A.; Johnson, W. T.; Broderick, C. L.; Montrose, C. R.; Brozinick, J. T.; Misener, E. A.; Bean, J. S.; Bensch, W. R.; Brooks, D. A.; Shuker, A. J.; Rito, C. J.; McCarthy, J. R.; Ardecky, R. J.; Tyhonas, J. S.; Dana, S. L.; Bilakovics, J. M.; Paterniti, J. R., Jr.; Ogilvie, K. M.; Liu, S.; Kauffman, R. F. A Tailored Therapy for the Metabolic Syndrome, The Dual Peroxisome Proliferator-Activated Receptor- α/γ Agonist LY465608 Ameliorates Insulin Resistance and Diabetic Hyperglycemia While Improving Cardiovascular Risk Factors in Preclinical Models. *Diabetes* **2002**, *51*, 1083–1087.

- (17) Saad, M. F.; Osel, K.; Lewin, A. J.; Patel, N.; Edwards, C. R.; Greco, S. Nunez, M.; Huang, W.-C.; Reinhardt, R. R. Ragaglitazar Improves Lipid Profile and Glycemic Control in Hypertriglyceridemic Type 2 Diabetes. *Diabetes* **2002**, *51* (Suppl. 2), A35–A36.
- (18) Strand, J.; Sandeman, D.; Skovsted, B.; Edsberg, B.; Müller, P. Ragaglitazar (NNC 61-0029, (-)DRF 2725): The Efficacy and Safety of a Novel Dual PPAR α and PPAR γ Agonist in Patients with Type 2 Diabetes. *Diabetes* **2002**, *51* (Suppl. 2), A141–A142.
- (19) Ebdrup, S.; Deussen, H.-J.; Zundel, M. Process for the preparation of substituted 3-phenyl-propanoic acid esters and substituted 3-phenyl-propanoic acids. PCT Appl. WO 0111072, 2001.
- (20) Deussen, H. J.; Zundel, M.; Valdois, M.; Lehmann, S. V.; Weil, V.; Hjort, C. M.; Østergaard, P. R.; Marcussen, E.; Ebdrup, S. Process development on the enantioselective enzymatic hydrolyses of the (*S*)-ethyl 2-ethoxy-3-(4-hydroxyphenyl)propanoate. *Org. Proc. Res. Dev.* **2003**, *7*, 82–88.
- (21) Grell, W.; Machleidt, H. PO-Aktivierete Alkoxylofinierung. *Justus Liebigs Ann. Chem.* **1966**, 53–67.
- (22) Wadsworth, W. S., Jr. Synthetic Applications of Phosphoryl-Stabilized Anions. *Org. React.* **1977**, *25*, 73–253.
- (23) Linde, H. Untersuchungen an Phenoxazinderivaten. *Arch. Pharm. Ber. Dtsch. Pharm. Ges.* **1960**, *293*, 537–542.
- (24) Cauquil, G.; Casadevall, A.; Casadevall, E. Recherches dans la série de la phenothiazine (3^e mémoire) Reaction de metallation (Research in the phenothiazine series (part 3). Metalation reaction). *Bull. Soc. Chim. Fr.* **1960**, 1049–1066.
- (25) Kim, S. H.; Martin, A. R. Tetracyclic Phenothiazines IV (1). Synthesis of 1,2,3,4-Tetrahydrozepino[3,2,1-*kl*]phenothiazine-4-one. *J. Heterocycl. Chem.* **1978**, *15*, 1503–1504.
- (26) Nygaard, L.; Wiede, P.; Jensen, A. F.; Olsen, H.; Ebdrup, S. Unpublished results.
- (27) *SHELXTL. Software package for single crystal structure determination*, version 5.1; Bruker AXS, Inc.: Madison, WI, 1997.
- (28) Crystallographic data for the structure has been deposited with the Cambridge Crystallographic Data Centre as Supplementary Publication No. CCDC 197689. Copies of the data can be obtained free of charge on application to CCDC, 12 Union Road, Cambridge CB2 1EZ, U.K. or on e-mail, deposit@ccdc.ac.uk.
- (29) Nicols, J. S.; Parks, D. J.; Conslor, T. G.; Blanchard, S. G. Development of a Scintillation Proximity Assay for Peroxisome Proliferator-Activation. *Anal. Biochem.* **1998**, *258*, 112–119.
- (30) Skrumsager, B. K.; Nielsen, K. K.; Pedersen, P. C. NNC 61-0029 ((-)-DRF2725): The multiple dose pharmacokinetics of a novel dual acting PPAR α and PPAR γ agonist in healthy subjects and type 2 diabetic patients. *Diabetes* **2001**, *50* (Suppl. 2), A123–A132.
- (31) Skrumsager, B. K.; Nielsen, K. K.; Reinhardt, R.; Pedersen, P. C. NNC 61-0029 ((-)-DRF2725): The single dose pharmacokinetics of a novel dual acting PPAR α and PPAR γ agonist in caucasian and Japanese healthy subjects. *Diabetes* **2001**, *50* (Suppl. 2), A445.
- (32) Nolte, R. T.; Wisely, G. B.; Westin, S.; Cobb, J. E.; Lambert, M. H.; Kurokawa, R.; Rosenfeld, M. G.; Willson, T. M.; Glass, C. K.; Milburn, M. V. Ligand binding and co-activator assembly of the peroxisome proliferator-activated receptor- γ . *Nature* **1998**, *395*, 137–143.
- (33) Uppenberg, J.; Svensson, C.; Jaki, M.; Bertilsson, G.; Jendeborg, L.; Berkenstam, A. Crystal Structure of the Ligand Binding Domain of the Human Nuclear Receptor PPAR γ . *J. Biol. Chem.* **1998**, *273*, 31108–31112.
- (34) Oberfield, J. L.; Collins, J. L.; Holmes, C. P.; Goreham, D. M.; Cooper, J. P.; Cobb, J. E.; Lenhard, J. M.; Hull-Ryde, E. A.; Mohr, C. P.; Blanchard, S. G.; Parks, D. J.; Moore, L. B.; Lehmann, J. M.; Plunket, K.; Miller, A. B.; Milburn, M. V.; Kliewer, S. A.; Willson, T. M. A peroxisome proliferator-activated receptor gamma ligand inhibits adipocyte differentiation. *Proc. Natl. Acad. Sci. U.S.A.* **1999**, *96*, 6102–6106.
- (35) Xu, H. E.; Lambert, M. H.; Montana, V. G.; Parks, D. J.; Blanchard, S. G.; Brown, P. J.; Sternbach, D. D.; Lehman, J. M.; Wisely, G. B.; Willson, T. M.; Kliewer, S. A.; Milburn, M. V. Molecular Recognition of Fatty Acids by Peroxisome Proliferator-Activated Receptors. *Mol. Cell* **1999**, *3*, 397–403.
- (36) Goodford, P. J. A computational procedure for determining energetically favorable binding sites on biologically important macromolecules. *J. Med. Chem.* **1985**, *28*, 849–857.
- (37) Boobbyer, D. N. A.; Goodford, P. J.; McWhinnie, P. M.; Wade, R. C. New hydrogen-bond potentials for use in determining energetically favorable binding sites on molecules of known structure. *J. Med. Chem.* **1989**, *32*, 1083–1094.
- (38) Wade, R. C.; Goodford, P. J. Further development of hydrogen bond functions for use in determining energetically favorable binding sites on molecules of known structure. 2. Ligand probe groups with the ability to form more than two hydrogen bonds. *J. Med. Chem.* **1993**, *36*, 148–156.
- (39) Molecular Discovery Ltd., 20a Berkeley Street, Mayfair, London W1X 5AE, U.K.
- (40) Oliver, W. R.; Shenk, J. L.; Snaith, M. R.; Russel, C. S.; Plunket, K. D.; Bodkin, N. L.; Lewis, M. C.; Winegar, D. A.; Sznajdman, M. L.; Lambert, M. H.; Xu, H. E.; Sternbach, D. D.; Kliewer, S. A.; Hansen, B. C.; Willson, T. M. A selective peroxisome proliferator-activated receptor γ agonist promotes reverse cholesterol transport. *Proc. Natl. Acad. Sci. U.S.A.* **2001**, *98*, 5306–5311.
- (41) Rarey, M.; Kramer, B.; Lengauer, T.; Klebe, G. A Fast Docking Method Using an Incremental Construction Algorithm. *J. Mol. Biol.* **1996**, *261*, 470–489.
- (42) Kramer, B.; Rarey, M.; Lengauer, L. Evaluation of the FlexX incremental construction algorithm for protein–ligand docking. *Proteins: Struct., Funct., Genet.* **1999**, *37*, 228–241.
- (43) Rarey, M.; Wefing, S.; Lengauer, T. Placement of medium-sized molecular fragments into active sites of proteins. *J. Comput.-Aided Mol. Des.* **1996**, *10*, 41–54.
- (44) Rarey, M.; Kramer, B.; Lengauer, T. Multiple automatic base selection: Protein–ligand docking based on incremental construction without manual intervention. *J. Comput.-Aided Mol. Des.* **1997**, *11*, 369–384.
- (45) Clark, R. D.; Strizhev, A.; Leonard, J. M.; Blake, J. F.; Matthew, J. B. Consensus scoring for ligand/protein interactions. *J. Mol. Graphics Modell.* **2002**, *20*, 281–295.
- (46) The enantiomeric purity can be significantly increased by diastereomer crystallization with (–)-ephedrine.
- (47) Cerenius, Y.; Stahl, K.; Svensson, L. A.; Ursby, T.; Oskarsson, A.; Albertsson, J.; Liljas, A. The crystallography beamline I711 at MAX II. *J. Synchrotron Radiat.* **2000**, *7*, 203–208.
- (48) Otwinowski, Z.; Minor, W. Processing of X-ray Diffraction Data Collected in Oscillation Mode. *Methods Enzymol.* **1997**, *276*, 307–326.
- (49) Collaborative Computational Project, N4. The CCP4 Suite: Programs for Protein Crystallography. *Acta Crystallogr.* **1994**, *D50*, 760–763.
- (50) Navaza, J. Amore—an automated package for molecular replacement. *Acta Crystallogr.* **1994**, *A50*, 157–163.
- (51) Brünger, A. T.; Kuriyan, J.; Karplus, M. Crystallographic R-factor refinement by molecular dynamics. *Science* **1987**, *235*, 458–460.
- (52) Brunger, A. T.; Adams, P. D.; Clore, G. M.; Delano, W. L.; Gros, P.; Grosse-Kunstleve, R. W.; Jiang, J.-S.; Kuszewski, J.; Nilges, M.; Pannu, N. S.; Read, R. J.; Rice, L. M.; Simonson, G. L.; Warren, T.; Badger, J.; Berard, D.; Kumar, R. A.; Szalma, S.; Yip, P.; Griesinger, C.; Junker, J. Crystallography and NMR System: A New Software Suite for Macromolecular Structure Determination. *Acta Crystallogr.* **1998**, *D54*, 905–921.
- (53) Kleywegt, G. J.; Jones, T. A. Databases in Protein Crystallography. *Acta Crystallogr.* **1998**, *D54*, 1119–1131.
- (54) SYBYL, version 6.8; Tripos Inc., 1699 South Hanley Road, St. Louis, Missouri, 63144.
- (55) Schrodinger Inc. (www.schrodinger.com).
- (56) Mohamadi, F.; Richards, N. G. J.; Guida, W. C.; Liskamp, R.; Lipton, M.; Cauffield, C.; Chang, G.; Hendrickson, T.; Still, W. C. MacroModel—An Integrated Software System for Modeling Organic and Bioorganic Molecules Using Molecular Mechanics. *J. Comput. Chem.* **1990**, *11*, 440–467.
- (57) Goodman, J. M.; Still, W. C. An Unbounded Systematic Search of Conformational Space. *J. Comput. Chem.* **1991**, *12*, 1110–1117.
- (58) Halgren, T. A. Merck Molecular Force Field. I. Basis, Form, Scope, Parametrization, and Performance of MMFF94. *J. Comput. Chem.* **1996**, *17*, 490–519.
- (59) Halgren, T. A. Merck Molecular Force Field. II. MMFF94 van der Waals and Electrostatic Parameters for Intermolecular Interactions. *J. Comput. Chem.* **1996**, *17*, 520–552.
- (60) Halgren, T. A. Merck Molecular Force Field. III. Molecular Geometries and Vibrational Frequencies for MMFF94. *J. Comput. Chem.* **1996**, *17*, 553–586.
- (61) Halgren, T. A.; Nachbar, R. B. Merck Molecular Force Field. IV. Conformational Energies and Geometries for MMFF94. *J. Comput. Chem.* **1996**, *17*, 587–615.
- (62) Halgren, T. A. Merck Molecular Force Field. V. Extension of MMFF94 Using Experimental Data, Additional Computational Data, and Empirical Rules. *J. Comput. Chem.* **1996**, *17*, 616–641.
- (63) Halgren, T. A. MMFF VI. MMFF94s Option for Energy Minimization Studies. *J. Comput. Chem.* **1999**, *20*, 720–729.
- (64) Halgren, T. A. MMFF VII. Characterization of MMFF94, MMFF94s, and Other Widely Available Force Fields for Conformational Energies and for Intermolecular-Interaction Energies and Geometries. *J. Comput. Chem.* **1999**, *20*, 730–748.
- (65) Still, W. C.; Tempczyk, A.; Hawley, R. C.; Hendrickson, T. Semianalytical Treatment of Solvation for Molecular Mechanics and Dynamics. *J. Am. Chem. Soc.* **1990**, *112*, 6127–6129.
- (66) Kristensen, J. B.; Johansen, S. K.; Valsborg, J. S.; Martiny, L.; Foged, C. Unpublished results.
- (67) Johansen, S. K.; Martiny, L. Unpublished results.